Optimization of 3D Plasmonic Crystal Structures for Refractive Index Sensing

Joana Maria,[†] Tu T. Truong,[†] Jimin Yao,[†] Tae-Woo Lee,[||] Ralph G. Nuzzo,[†] Sven Leyffer,[§] Stephen K. Gray,*[,‡] and John A. Rogers*[,†]

Departments of Chemistry and Materials Sciences & Engineering and Frederick Seitz Materials Research Laboratory, University of Illinois, Urbana, Illinois 61801, Center for Computation & Technology, Louisiana State University, Baton Rouge, Louisiana 70803, Mathematics and Computer Science Division, Argonne National Laboratory, Argonne, Illinois 60439, and Center for Nanoscale Materials, Argonne National Laboratory, Argonne, Illinois 60439

Received: March 18, 2009; Revised Manuscript Received: April 17, 2009

We study the refractive index sensitive transmission of a 3D plasmonic crystal that consists of a square array of subwavelength cylindrical nanowells in a polymer conformally coated with a gold film. Using extensive 3D finite-difference time-domain simulations, we investigate the effect of system parameters such as periodicity, well diameter and depth, and metal thickness on its refractive index sensitivity. These theoretical results are also confirmed experimentally in some cases. Our calculations predict an enhancement in sensitivity by an order of magnitude when the plasmonic crystal characteristics are optimized.

1. Introduction

The optical properties of metallic nanostructures continue to be the focus of much research. Such systems, ranging from isolated metal nanoparticles to precisely fabricated arrays of metal nanoparticles and subwavelength apertures in metal films can exhibit strong optical responses near certain wavelengths often associated with surface plasmon excitations.[1−10] Surface plasmons are collective excitations of free electrons near metal surfaces that produce intense light localized near the metal surface. These "plasmonic" properties are relevant to chemical sensing applications.[8−10] Two well-established chemical sensing approaches making use of surface plasmons are the surface plasmon resonance (SPR) technique which involves thin metal films[9] and surface enhanced Raman scattering (SERS) on rough metal films or related structures.[10]

Recently, we have fabricated and characterized certain plasmonic crystal structures involving a polymer film with a pattern of imprinted wells on one side and a metal (gold) film deposited on the patterned side[1,11] As with the pioneering work of Ebbesen et al. on arrays of subwavelength wells in metal films,[12] these systems can exhibit very structured transmission spectra with peaks corresponding to a surprising amount of optical transmission. The plasmonic crystals we are considering are somewhat more complex in character, involving not just wells but well structures with metal also being deposited on the bottom and/or sidewalls of the original polymer well. This complexity provides additional system parameters that can be varied to fine-tune the optical response.

The optimization of system parameters for, say, refractive index (RI) sensing purposes is a challenging problem because there are a variety of variables such as the well diameter, depth, and metal thickness, to be considered. It is difficult to predict, based on simple physical principles involving the individual components, what the full system's optical response would be. However, rigorous electrodynamics simulations can be used for such purposes. In this work, we carry out extensive finite-difference time-domain (FDTD) modeling of the plasmonic crystal configuration of Figure 1 and compare the calculated results with experimental ones, where available. In particular, we predict how the figure-of-merit (FOM) for RI sensing can be increased by an order of magnitude with a suitable choice of system parameters.

2. Experimental and Computational Methods

Materials. Poly dimethylsiloxane (soft PDMS; Dow Corning, Sylgard 184) was purchased from Ellsworth Adhesives. The components[13] used in the hard PDMS formulation were purchased from Gelest. Photocurable polyurethane (PU; NOA73) was purchased from Norland Products. All reagents were used as received without further purification. Polyethylene glycol buffer solutions (PEG) (0−7.6 wt %) were prepared with 18 MΩ deionized water (Millpore Milli-Q Academic A-10 system).

3D Plasmonic Crystal Fabrication. Soft nanoimprint lithography on an NOA layer with composite h-PDMS/s-PDMS molds[14] in the geometry of square arrays of cylindrical posts was used to fabricate patterned relief structures of nanowells[1,15] A continuous layer of gold was deposited on the embossed NOA by sputter deposition in 5 mTorr Ar (ATC 2000, AJA International).

Transmission-Mode Spectrophotometry. All optical transmission measurements of the 3D plasmonic crystals were carried out on a Varian 5G UV−vis−NIR, operating in normal incidence transmission mode. Solutions were injected into a flow cell built around the plasmonic crystal using a syringe pump at a rate of 0.1 mL/min.

FDTD Calculations. The finite-difference time-domain (FDTD) method was used to model the optical properties of the 3D plasmonic crystals.[16,17] In this approach, the electric and magnetic fields describing light interacting with the system are propagated in time according to Maxwell's equations, and relevant observables such as the zero-order transmitted light are inferred. A single unit cell is considered, with appropriate

* To whom correspondence should be addressed. E-mail: gray@anl.gov, jrogers@uiuc.edu.
[†] University of Illinois.
[||] Center for Computation & Technology, Louisiana State University.
[§] Mathematics and Computer Science Division, Argonne National Laboratory.
[‡] Center for Nanoscale Materials, Argonne National Laboratory.

10.1021/jp9024552 CCC: $40.75
Published on Web 05/21/2009

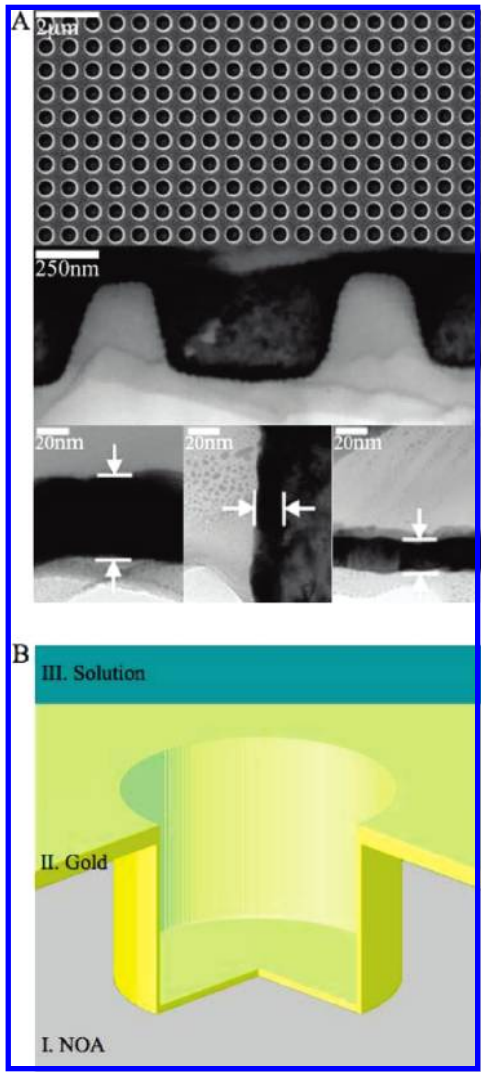

Figure 1. (A) (Top frame) Scanning electron micrograph (SEM) of a 3D plasmonic crystal with a periodicity of 748 nm, a well diameter of 456 nm, and a relief or well depth of 350 nm. (Middle frame) Cross-section transmission electron micrograph (TEM) of the plasmonic crystal showing the polymer nanowell array surface in white covered by a continuous gold layer in black. (Bottom frame) High magnification TEM images showing the gold thickness at the top (~35 nm; left), sidewall (~12 nm; middle) and bottom (~20 nm; right) of the nanowell array. (B) Schematic representation of the unit cell used in the computational electrodynamics modeling. Light is incident from Region I and propagates in the direction of the gold layer that constitutes Region II. The transmission spectra are obtained in Region III.

periodic boundary conditions to describe an infinite square array, and uniaxial perfectly matching layers[16] at the z grid boundaries are used to absorb the outgoing field components. The computational domain consists of a square of $P/\Delta x \times P/\Delta y$ grid points centered on the nanowell (P is the grating periodicity in nm) in the $x-y$ plane and 750 grid points in z, with a resolution of $\Delta x = \Delta y = \Delta z = 4$ nm. Each calculation is carried out for a total simulation time of 150 fs. Test calculations with smaller grid spacings and larger simulation times indicated that the results are converged. The initial excitation of the system by a time-windowed plane wave is carried out using a total field/scattered field formulation[16] with boundary 600 nm below the bottom surface of the film. The materials are defined by assigning to spatial regions, where they occur, appropriate relative dielectric constants, ε_R, or equivalently, refractive index $n = \varepsilon_R^{1/2}$. We use: $n = 1.56$ for NOA; $n = 1.332$ for water; $n = 1.3336$, 1.3357, and 1.3377 for the 1.4, 2.8, and 4.2 wt % PEG solutions, respectively. In the case of gold, it is important to include its wavelength dependence, $\varepsilon_R = \varepsilon_{Au}(\lambda)$. This is described by a Drude plus two-pole Lorentz representation with parameters fit[16−19] to match experimental permittivity data[20] over the range 400−1000 nm. The Drude parameters are $\varepsilon_\infty = 5.40$, $\gamma_D = 0.1077 \times 10^{15}$ Hz and $\omega_D = 0.1331 \times 10^{17}$ Hz and Lorentz parameters are $\omega_{L1} = 0.4897 \times 10^{16}$ Hz and $\omega_{L2} = 0.4147 \times 10^{16}$ Hz, $\gamma_{L1} = 0.4358 \times 10^{15}$ Hz and $\gamma_{L2} = 0.4175 \times 10^{15}$ Hz, $g_{L1} = 0.6011$ and $g_{L2} = 0.3989$, and $\Delta\varepsilon = 1.8094$. An auxiliary differential equations approach, which introduces additional polarization vectors that are equivalent to the Drude−Lorentz model, is then employed.[16,19] The zero-order transmission is obtained by calculating the flux of the electromagnetic energy through the $x-y$ plane $z_T = 800$ nm above the top surface of the film, and normalizing it with the appropriate incident flux. Note that in order to obtain just the zero-order (or zero angle of deflection) contribution, the electric and magnetic fields in the flux or Poynting vector must be first averaged over the x-y plane as discussed in ref 21.

Owing to the large 3D grids required to describe the system, a typical FDTD calculation with parameters as described above can require up to 6 h of clock time running on 128 (2 GHz) processors of a parallel computer.

3. Results and Discussion

A set of plasmonic crystals with periodicities ranging from 400 to 1152 nm, diameters from 156 to 456 nm, relief or well depths from 300 to 600 nm and well film thickness from 0 to 150 nm were studied both theoretically and, in some cases, experimentally. The basic system structure (Figure 1) is that of ref[1] It differs from that of our first plasmonic crystal structure[11] in that there is a conformal coating of metal formed by sputter deposition over the embossed polymer side. The quasi-3D plasmonic crystal was formed by depositing a metal by electron beam (ebeam) evaporation, which created a gold nanowell array with a separate level of disks in the bottom of the embossed nanowells. The new structure was found to be somewhat more sensitive, particularly in the visible, than the original structure, which had very little metal on the nanowell sidewalls consisting mainly of a pileup of gold grains around the disks at the bottom of the nanowells.[11]

For the experiments, large area and spatially uniform square arrays of cylindrical nanowells were embossed in a polymer by soft nanoimprint lithography and a thin continuous layer of gold was deposited by sputter deposition at ~5 mTorr to complete the plasmonic crystal fabrication process. The top frame of Figure 1(A) shows a scanning electron microscopy (SEM) image of a plasmonic crystal with periodicity of 748 nm and a well diameter and well depth of 456 and 350 nm, respectively. The middle frame of Figure 1(A) shows a transmission electron microscopy (TEM) image of the same plasmonic crystal. This image, together with the TEM images on the bottom frame of Figure 1(A), allows the characterization of the gold layer geometry. A gold thickness of 35 nm on the top of crystal, 12 nm on the sidewall, and 20 nm on the bottom of the nanowells was measured. Figure 1(B) shows a schematic diagram of the unit cell used in the modeling; Region I represents the polymer, Region II consists of the gold geometry as inferred from the TEM images, and Region III represents a region of variable index of refraction, e.g., water or a polyethylene glycol (PEG) solution. The plane wave is launched from region I (NOA) and the transmission spectrum is calculated in Region III (the solution).

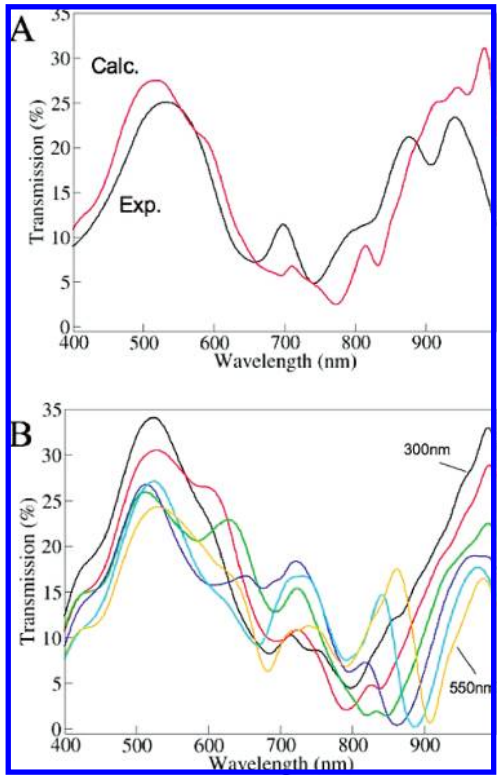

Figure 2. (A) Experimental (black) and calculated (red) normal incidence transmission spectra in water for a plasmonic crystal with a periodicity of 748 nm, diameter of 456 nm, and relief depth of 350 nm. (B) Calculated normal incidence spectra in water of a series of plasmonic crystals with a periodicity of 752 nm; hole diameter of 456 nm; and relief depths of 300 nm (black), 350 nm (red), 400 nm (green), 450 nm (blue), 500 nm (cyan), and 550 nm (orange), respectively. For the calculated results in (A) and (B), the gold thickness is 32 nm on the top, 16 nm on the bottom, and 8 nm on the sidewalls.

3.1. Relief Depth. Figure 2(A) shows the experimental and FDTD calculated normal incidence transmission spectra for the sample of Figure 1(A) when in contact with water. The periodicity, diameter, and relief (or well) depth for this base system are 748, 456, and 350 nm, respectively. Owing to our grid resolution (4 nm), it is not possible to exactly match the various gold layer thicknesses in Figure 1(A). Instead, the theoretical calculations employ top, bottom, and sidewall thicknesses of 32, 16, and 8 nm, respectively. The calculated spectrum captures the main experimental spectral features, although some differences start to be noticeable in the longer wavelength region. This can probably be explained by the fact that the full 3D FDTD calculations did not include the water absorption effect, which becomes important for $\lambda > 1000$ nm. The peak structure near 500 nm corresponds to the background thin film transmission. Other peak structures, as in previous work,[1,11,17] are due to local surface plasmon (LSP) resonances associated with nanowells and Bloch wave surface plasmon polaritons (BW-SPPs), which are standing waves formed from counter-propagating surface plasmon polaritons. Fourier transforms of the time-evolving electric fields from our calculations on specific frequencies can yield information about the character of the resonances. In the present examples it turns out that it is difficult to find isolated BW-SPPs and that most peaks are LSPs or combinations of LSPs and BW-SPPs with a strong LSP character.

Figure 2(B) shows calculated normal incidence spectra for a series of plasmonic crystal samples with the same periodicity (752 nm), well diameter (456 nm), and gold thickness (32 nm on the top, 16 nm on the bottom, and 8 nm on the nanowell sidewalls) as a function of the nanowell relief depth. The resonances at 697 and 794 nm get more intense as the relief depth increases, which can be explained by a stronger interaction between the gold top surface and the gold disk at the bottom of the nanowell. To investigate how these changes in the plasmon resonances with relief depth affect the plasmonic crystals sensitivity, FDTD calculations were carried out for the series of plasmonic crystals in contact with solutions of increasing refractive index.

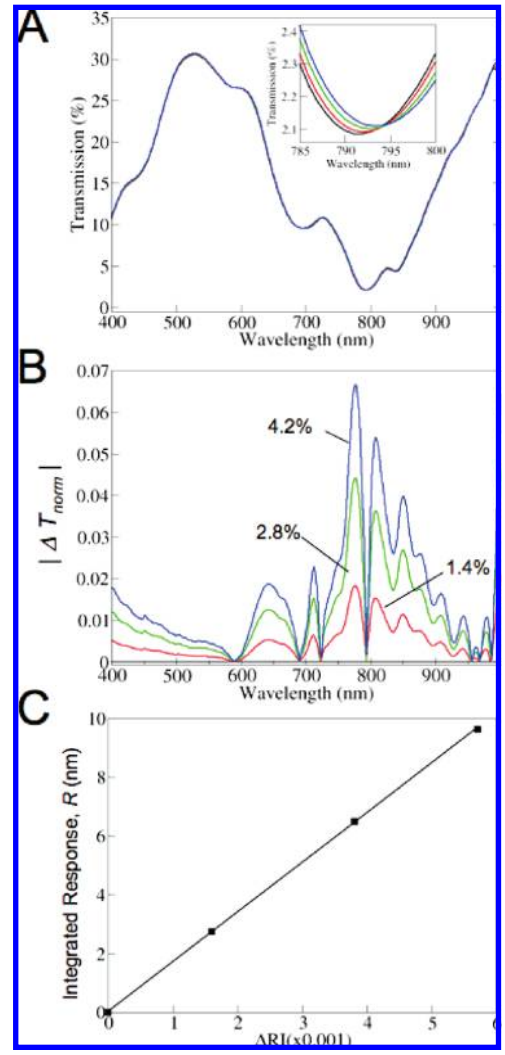

Figure 3. (A) Calculated normal incidence transmission spectra of the configuration described in the caption of Figure 2(B), with relief depth 350 nm, for different refractive index environments in Region III: water (black line), 1.4 wt % PEG solution (red line), 2.8 wt % PEG solution (green line), and 4.2 wt % PEG solution (blue line). Inset: Magnification of the transmission spectra for wavelengths near ~790 nm. (B) Plot of normalized difference transmission spectra calculated using the results from (A) referenced to the transmission spectrum in water (see eq 1). (C) Plot of the total response of the plasmonic crystal over all wavelengths as a function of the change in refractive index of the PEG solution. This plasmonic crystal, which we take to be our base system upon which to improve upon, exhibits a FOM ≈ 1700 nm/RIU corresponding to the slope of the curve in (C).

Figure 3(A) shows the obtained normal incidence transmission spectra for a plasmonic crystal of 350 nm relief depth for solutions with known RI values ranging from 1.332 to 1.3377, corresponding to %PEG concentrations ranging from 0 to 4.2 wt %. On the scale of this figure, it is not possible to discern the transmission changes with RI. However, the inset of Figure

3(A), depicting a 15 nm region near a minimum, shows that spectral features do shift in position and magnitude. Such small changes, if of good fidelity, are indeed used for RI sensing.[22−25] Recently, however, it was found that a multispectral analysis that accounts for both the wavelength and intensity-based changes in the transmission spectra is more appropriate for imaging applications with our type of plasmonic crystal.[1,11] In this work, we use this latter approach and calculate the total response of the plasmonic crystal over all wavelengths with

$$R = \int |\Delta T_{\text{norm}}| d\lambda = \int \left| \frac{T_{\text{solution}} - T_{\text{baseline}}}{T_{\text{baseline}}} \right| d\lambda \quad (1)$$

In eq 1, T_{solution} is the observed transmission for a given solution composed of solvent (water) and PEG solute, and the baseline transmission, T_{baseline}, is the transmission by the plasmonic crystal in pure solvent (water). The integrand of eq 1 is the normalized change in transmission relative to the pure solvent.

Some additional remarks should be made concerning eq 1. Contrary to resonance wavelength based senors, for example, the sensitivity response of eq 1 might actually improve in the case of broad resonances. A limiting feature of eq 1, however, is that if T_{baseline} is small compared to the absolute changes in transmission, the result might be overly sensitive to T_{baseline}.

Figure 3(B) shows that this normalized transmission difference, ΔT_{norm}, is much more sensitive to the RI of the solution. Figure 3(C) shows the calculated total response as a function, R, as a function of solution RI. In general, for the small RI changes, this response is well approximated by a line. The slope of this line is what we take to be the figure of merit (FOM). In this example, FOM $\approx$ 1700 nm/RIU, and we will take this FOM to be the base FOM upon which to improve upon. Two points should be about eq 1, and the FOM values we infer from its variation with RI. First, while the FOM has units of nm/RIU, it should not be confused with a spectral resonance position shift with RIU. The nm units arise from integration of the response over the 400−1000 nm visible−near IR wavelength range of interest. The second point is that ref 1 used a response measure of just the magnitude of the transmission difference, as opposed to the normalized transmission difference used in eq 1. Given that it can be difficult to achieve quantitative agreement between modeling and experimental results in these complex systems, we anticipate that use of a relative measure might factor out some experimental and theoretical differences and lead to more comparable FOM values. (The present FOM = 1700 nm/RIU for our base plasmonic crystal system corresponds to the value of the older FOM of 6000 Δ%T/RIU that was reported in ref 1).

The same procedure as above was followed to calculate the bulk refractive index sensitivity of plasmonic crystals with relief depths ranging from 300 to 600 nm, and the results are shown in Figure 4. The sensitivity increases with relief depth until a maximum sensitivity of 3354 nm/RIU is achieved for a relief depth of 500 nm after which the sensitivity starts to decrease indicating that there is an optimum relief depth for the interaction between the top metal layer and the gold disks at the bottom of the nanowell. Figure 4 also presents results for an experimental study of the sensitivity as a function of relief depth for depths between 300 and 500 nm that also show an increase in the plasmonic crystal sensitivity. Unfortunately, it was not possible to obtain larger relief depths than 500 nm to verify that there is a maximum in this region. While the magnitudes of the experimentally determined FOMs are comparable to the theoretical ones, they can be smaller by a factor of 2 owing presumably to various imperfections such as nonuniform metal layer thicknesses.

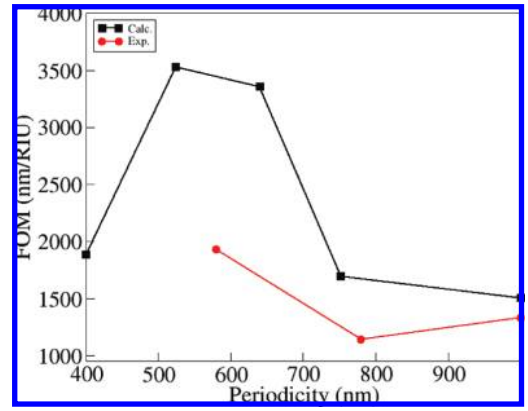

Figure 4. Calculated sensitivity or figure of merit (FOM) for a series of plasmonic crystals with configuration as described in the caption of Figure 2(B) but for varying relief depth (solid black squares connected by black lines). The sensitivity is highest for a relief depth of ~500 nm. Available experimental results for the relief depth dependence of plasmonic crystals with comparable configurations are also shown (solid red circles connected by red lines).

3.2. Periodicity and Diameter. A series of plasmonic crystal samples with the same nanowell well diameter (456 nm), relief depth (350 nm), and gold thickness (32 nm on the top, 16 nm on the bottom and 8 nm on the nanowell sidewalls) but with periodicities varying between 552 nm and 1152 nm were modeled. The FOM for bulk refractive index sensitivity is ~2100 nm/RIU for a periodicity of 552 nm and it decreases, in an approximately linear manner, as the periodicity increases [Supporting Information, Figure S1(A)], indicating an enhanced coupling between neighborhood nanowells as the distance between nanowells decreases (equivalent to decreasing the periodicity) that causes an increase in the LSP intensities.[26−28] By periodicity 1152 nm, the FOM is ~550 nm/RIU.

Increasing the well diameter for a fixed periodicity can have a similar effect to decreasing the periodicity since well-to-well interactions also increase. We carried out FDTD calculations for a constant plasmonic crystal periodicity of 752 nm and increased the well diameter between 156 and 456 nm [Supporting Information, Figure S1(B)]. The FOM for bulk refractive index sensitivity ranged from ~800 nm/RIU at diameter 156 nm to ~1700 nm/RIU at diameter 456 nm.

Simultaneously varying the periodicity and diameter has a less straightforward effect. The above results might suggest that simultaneously decreasing the periodicity and increasing the well diameter would lead to higher FOM values. However, our best results with the individual variations are already near the physical limit of what is possible without the system no longer consisting of nonoverlapping wells. Instead, we chose to investigate the opposite limit of increasing the diameter with decreasing periodicity or, equivalently, decreasing the diameter with increasing periodicity. Figure 5 shows results of calculations for when both the plasmonic crystal periodicity and well diameter are changed with the diameter being taken to be 0.6 times the periodicity. Interestingly, a maximum sensitivity of ~3500 nm/RIU is achieved for a periodicity of 524 nm and a well diameter of 320 nm, which is 75% better than our best result concerning individual variations. Figure 5 also shows experimental results for plasmonic crystals with comparable periodicity and diameter variations. As with our other comparisons with the modeling results, the experimental FOM shows

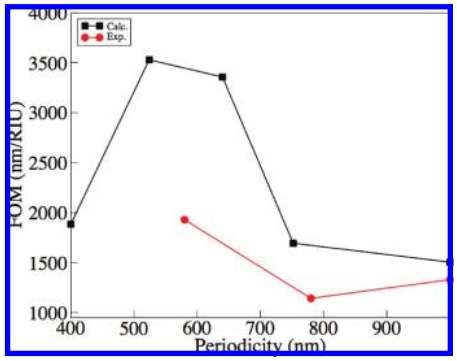

Figure 5. Simultaneous variation of periodicity and well diameter. The diameter is taken to be 0.6× the corresponding periodicity. The calculated results have fixed relief depth 350 nm, and top, bottom, and sidewall gold thicknesses of 32, 16, and 8 nm, respectively (black squares connected by black lines). Available experimental results for comparable systems are also plotted (solid red circles connected by red lines).

similar gross trends and is comparable in magnitude but up to twice as small. Unfortunately, experimental limitations prevented us from investigating the lower periodicity and diameter values and confirm the theoretical prediction of a maximum in the FOM.

Notice that the experimental FOM in Figure 5 increases slightly as the periodicity increases from 780 to 1000 nm, which is not seen in the calculated results. SEM images of the plasmonic crystal samples (not shown here) showed that the nanowells for a periodicity of 580 and 780 nm are cylindrical, while for a periodicity of 1000 nm, they are rectangular. It is expected that sharper geometries will induce stronger LSP resonances, which can possibly explain the increase in sensitivity for this periodicity.

3.3. Gold Film Thickness. Finally, the effect of the gold thickness on the top, sidewalls and bottom of the nanowells is considered. FDTD calculations show that by keeping the sidewall and bottom gold thicknesses (8 nm and 16 nm, respectively) and changing the top gold thickness, an increase in sensitivity with top gold thickness was seen until it reached a maximum of ∼3100 nm/RIU for a top gold thickness of 64 nm, for which afterward it started to decrease [Supporting Information, Figure S2(A)]. This result is not surprising since it is well know that there is an optimal thickness to couple into the plasmons on a thin metal film that depend on the wavelength and materials involved. For a thin gold film in contact with a prism and air and wavelengths between 600 and 1000 nm, the optimum coupling thickness varies between 44 and 50 nm.[9,29]

When the sidewall gold thickness is changed and the top and bottom gold thicknesses are kept the same (32 nm and 16 nm, respectively), the sensitivity increases with gold thickness until a maximum sensitivity of ∼5400 nm/RIU is reached for a sidewall gold thickness of 96 nm after which the sensitivity begins to decrease [Supporting Information, Figure S2(B)]. From classical Mie theory, it is well know that LSP resonances are extremely sensitive to the size and shape of nanoparticles and nanowells.[8,30] By keeping the nanowell diameter the same and changing the sidewall gold thickness, we are effectively changing the well diameter size and the sidewall gold thickness of 96 nm corresponds to an optimum separation between nanowells.

The effect of the bottom gold thickness [Supporting Information, Figure S2(B)], when keeping the top and sidewall thickness constant (32 nm and 8 nm, respectively), on the bulk refractive index sensitivity is not as large as that with the sidewall gold thickness, since LSP resonances are not as sensitive to the bottom gold thickness as they are to the nanowell well diameter.

3.4. Optimized Structures. Owing to the large computational effort associated with just one simulation (see Sec. 2), a full optimization of all of the system parameters to maximize the bulk refractive index sensitivity is difficult to achieve. We decided instead to optimize aspects of the metal thickness in relation to (i) our optimized relief depth result of Sec. 3.1 and (ii) our optimized simultaneous periodicity-diameter result of Sec. 3.2. On the basis of the latter result, a more systematic optimization procedure is then used to obtain our best estimate for an optimum structure.

Section 3.1 showed, for periodicity 752 nm and diameter 456 nm (these parameters are close to the ones reported in ref 1), that a relief depth of ∼500 nm is optimal. If we take this configuration, but use the optimal gold layer thicknesses inferred in Sec. 3.3 above, 64 nm of gold on the top surface, 96 nm of gold on the nanowell sidewalls, and 24 nm on the bottom surface, we obtain from our FDTD calculations a sensitivity of ∼6800 nm/RIU. This result is ∼4× higher than the reported sensitivity in ref[1] Although the FDTD calculations allowed us to optimize the plasmonic crystal sensitivity the resulting gold geometry cannot be easily implemented experimentally. For simplicity, we also investigated use of a uniform gold layer, i.e. the same top layer, bottom layer and wall thickness. (By sputtering gold onto the crystal at an increased pressure, such a uniform gold geometry could possibly be achieved.) Calculations were carried out to determine to optimal gold thickness for this case. Figure 6(A) shows that a calculated maximum sensitivity of ≈ 4400 nm/RIU occurs for a uniform gold thickness of ≈ 96 nm. This sensitivity is ≈ 3 times higher than the reported calculated sensitivity in ref.[1] The calculated trends in sensitivity as a function of gold thickness were also verified experimentally as is shown in Figure 6(B). We should note that the experimental results in Figure 6(B) do not involve the same gold thickness for top, bottom and sidewall layers but correspond to the proportions consistent with Figure 1(A), with the horizontal axis in Figure 6(B) corresponding to the top layer thickness.

When considering the simultaneous variation of periodicity and diameter in Sec. 3.2 [e.g., Figure 3(A)] it was shown that a relatively large sensitivity can be obtained for a plasmonic crystal with a periodicity of 524 nm and a well diameter of 320 nm. For simplicity we continue to use a uniform gold layer in our calculations and consider variation of the FOM with its thickness in Figure 6(C). An impressive maximum sensitivity of ≈ 16,600 nm/RIU is obtained for a gold thickness of 96 nm, which is a factor ≈ 10 times higher than the calculated sensitivity reported in ref 1. Note that these latter calculations were actually carried out with a relief depth of 400 nm, which is slightly larger by 50 nm than that used in Sec. 3.2. A more rigorous attempt at finding a true maximum of the FOM with respect to the relevant parameters now follows.

While informative, the above systematic variations of the various system parameters may not lead to the most optimal sensitivity. Unfortunately, the complex interplay between system parameters that we have seen above makes it difficult to proceed on simple physical grounds. An alternative is to employ optimization techniques to maximize the figure of merit. However, we cannot apply gradient-based optimization methods, because the FDTD simulations preclude the accurate and efficient computation of derivatives. Thus, we consider using derivative-free optimization, see, e.g., Conn et al. [31] We therefore build a surrogate model of our simulation results and use this

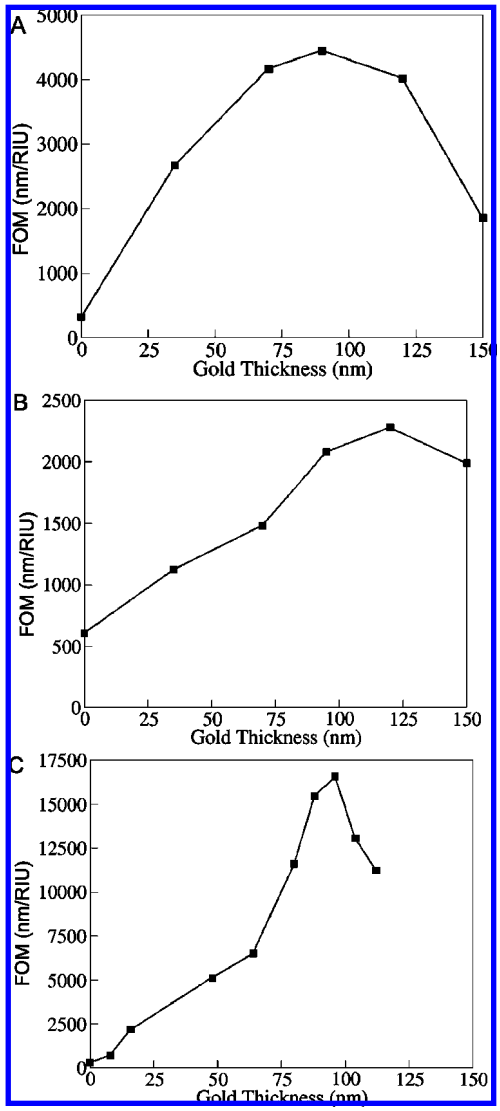

Figure 6. (A) Calculated FOM for the plasmonic crystal assuming a uniform thickness gold layer covering the nanowell array. (B) Experimental FOM for varying the top gold layer thickness with the bottom and sidewall thicknesses being in proportions relative to the top layer similar to Figure 1(A). (C) Calculated FOM for a series of plasmonic crystals with periodicity 524 nm, well diameter 320 nm, relief depth 400 nm, and a uniform gold layer.

model to predict the parameter values that lead to the optimal sensitivity. This process is iterative in character since simulations are run at the predicted optimal points of the surrogate and the new simulation result is used to refine the surrogate model and make further predictions. We consider a system parameter vector $x = (x_1, x_2, x_3, x_4)^T$, where x_1 is the well depth, x_2 is the periodicity, x_3 is the relief depth, and x_4 is uniform metal layer thickness. Given a current iterate $x^{(k)}$, the sensitivity is then approximated by a quadratic function of the form $q(x) = q_0 + g^T x + x^T W x/2$ within a trust-region around the current best parameter vector, denoted by $|| x^{(k)} - x || \leq \Delta_k$, where Δ_k is the trust-region radius and ||... || denotes the Euclidean norm. Here, q_0 is a scalar, g is a vector, and W is a symmetric matrix representing second-order information, and the superscript T means transposition. The quadratic surrogate, $q(x)$, has 15 parameters (q_0, g, and W), which we fit to our available data. We follow Powell[32] and compute a least-change Hessian interpolation. Initially, we use a subset of the data points generated during the coordinate-wise search. At every iteration, the surrogate predicts a new maximum, and we run the FDTD simulations to obtain the actual sensitivity at this maximum. If the new point improves the FOM, then we move to this new point, and recenter the trust-region. Otherwise, we exploit the new value to improve the surrogate model, by adding this value to the data from which we fit the quadratic.

After eight iterations, we were able to find a new optimal sensitivity of 18 700 nm/RIU, which is a 13% improvement over the result in Figure 6(C). This new optimum corresponds to x/nm = (330, 530, 419, 100), whereas the point in Figure 6(C) corresponds to x/nm = (320, 524, 400, 96). We continued to run the derivative-free optimization solver for another 10 iterations without any further improvement.

We believe that it is unlikely that we can discover a configuration with a significantly better FOM. The initial coordinate search implies that we have already covered much of the design space. The optimization routine is used to home-in on the most promising region, and it seems unlikely that other far-away points can improve the design. We interpret the fact that our local surrogate does not improve the FOM over 10 consecutive iterations as an indication that the design cannot be improved locally. We observe that the model does not settle down, because it contains one positive eigenvalue, which may be an artifact of the quadratic model we have chosen. To remove this eigenvalue and prove local optimality, we would have to run $3^4 = 81$ FDTD simulations, which is prohibitive. Finally, it is instructive to compare how our particular plasmonic crystal, involving conformal coating by metal of the nanowell structure, compares with other possible structures. The plasmonic crystal result of Figure 6(C) was therefore compared to the bulk refractive index sensitivity of plasmonic crystals with different gold structures but the same physical parameters. A crystal sample with no gold layer (i.e., just the imprinted polymer) is found to have a sensitivity of just 265 nm/RIU [Supporting Information, Figure S3]. This value reflects the contribution of Fresnel-type reflections to the calculated bulk refractive index sensitivity of our plasmonic crystal that is only 1.6% of the total calculated sensitivity. A plasmonic crystal with 96 nm of gold on the top surface and at the bottom of the nanowell—i.e., no gold on the sidewalls—has a sensitivity of ~14 800 nm/RIU [Supporting Information, Figure S4], showing that the sidewall gold thickness of our type of plasmonic crystal effectively increases the total sensitivity. A plasmonic crystal with 96 nm on the top surface only yields a sensitivity of ~7700 nm/RIU [Supporting Information, Figure S5], whereas a plasmonic crystal with 96 nm of gold on the bottom of the nanowell only yield a sensitivity of ~1300 nm/RIU, which are ~46% and 7.6% of the calculated maximum sensitivity, respectively. The effect of the gold disk at the bottom of the nanowell in the sensitivity is smaller than the effect of the top gold surface and the gold sidewalls as expected. The calculated result was also compared to the sensitivity of a plasmonic crystal with sub-wavelength wells in a 96 nm gold film. A sensitivity of ~6100, which is ~37% smaller than the calculated sensitivity of the optimal structure, was obtained.

4. Conclusions

We investigated how light transmission through 3D plasmonic crystals is influenced by the periodicity and diameter of the well structures and various metal layer thicknesses. In particular, we focused on optimizing a figure-of-merit (FOM) associated with the refractive index (RI) sensing capabilities of such systems. Our extensive finite-difference time-domain (FDTD) calculations revealed strong dependences that can be associated with

coupling into and out of surface plasmon excitations. In particular, variation of the metal film thicknesses associated with the nanowell sidewalls and bottom can lead to very large sensitivities. In some instances, we also provided experimental confirmation of the predicted trends. Furthermore, we demonstrated that by carefully optimizing the system parameters, the sensitivity can be enhanced by an order of magnitude. A number of system features need to be further studied both experimentally and theoretically in order to achieve even greater sensing capabilities. These include the role of nanowell shape (e.g., cylindrical vs rectangular), as well as the consideration of systems with longer wavelength plasmon resonances that might lead to stronger responses.

While we found reasonable qualitative agreement between our theoretical predictions and experimental results, it is of course desirable to achieve better quantitative agreement. This can be achieved by introducing imperfections into the theoretical model as in ref 11 and/or improved experimental fabrication. More precise experimental control of, in particular, the nanowell metal thickness coating will also be of utility in achieving better sensing capabilities. Future theoretical work will also be directed toward extending the derivative-free optimization approach[31,32] and investigating alternative optimization methods.

Acknowledgment. This work was carried out in part in the Frederick Seitz Materials Research Laboratory Central Facilities, University of Illinois, which is partially supported by the U.S. Department of Energy under Grant Nos. DE-FG02-07ER4653 and DE-FG02-07ER46471. The work at Argonne and use of the Center for Nanoscale Materials was supported by the U.S. Department of Energy, Office of Science, Office of Basic Energy Sciences, under Contract No. DE-AC02-06CH11357. The authors gratefully acknowledge use of the *Turing* cluster maintained and operated by the Computational Science and Engineering Program at the University of Illinois. *Turing* is a 1536-processor Apple G5 X-server cluster devoted to high performance computing in engineering and science.

Supporting Information Available: Five additional figures. This material is available free of charge via the Internet at http://pubs.acs.org.

References and Notes

(1) Yao, J.; Stewart, M. E.; Maria, J.; Lee, T.-W.; Gray, S. K.; Rogers, J. A.; Nuzzo, R. G. *Angew. Chem., Int. Ed.* **2008**, *47*, 5013–5017.
(2) Kelly, K. L.; Coronado, E.; Zhao, L. L.; Schatz, G. C. *J. Phys. Chem. B* **2003**, *107*, 668–677.
(3) Hutter, E.; Fendler, J. H. *Adv. Mater.* **2004**, *16*, 1685–1706.
(4) Lal, S.; Link, S.; Halas, N. J. *Nat. Photonics* **2007**, *1*, 641–648.
(5) Wang, H.; Brandl, D. W.; Nordlander, P.; Halas, N. J. *Acc. Chem. Res.* **2007**, *40*, 53–62.
(6) Liao, H. W.; Nehl, C. L.; Hafner, J. H. *Nanomedicine* **2006**, *1*, 201–208.
(7) Coe, J. V.; Heer, J. M.; Teeters-Kennedy, S.; Tian, H.; Rodriguez, K. R. *Annu. Rev. Phys. Chem.* **2008**, *59*, 179–202.
(8) Stewart, M. E.; Anderton, C. R.; Thompson, L. B.; Maria, J.; Gray, S. K.; Rogers, J. A.; Nuzzo, R. G. *Chem. Rev.* **2008**, *108*, 494–521.
(9) Homola, J. *Surface Plasmon Resonance Based Sensors*; Springer: Berlin, 2006.
(10) Stiles, P.; Dieringer, J.; Shah, N. C.; Duyne, R. P. V. *Ann. Rev. Anal. Chem.* **2008**, 1.
(11) Stewart, M. E.; Mack, N. H.; Malyarchuk, V.; Soares, J.; Lee, T. W.; Gray, S. K.; Nuzzo, R. G.; Rogers, J. A. *Proc. Natl. Acad. Sci., U.S.A.* **2006**, *103*, 17143–17148.
(12) Ebbesen, T. W.; Lezec, H. J.; Ghaemi, H. F.; Thio, T.; Wolff, P. A. *Nature* **1998**, *391*, 667–669.
(13) Hua, F.; Sun, Y. G.; Gaur, A.; Meitl, M. A.; Bilhaut, L.; Rotkina, L.; Wang, J. F.; Geil, P.; Shim, M.; Rogers, J. A.; Shim, A. *Nano Lett.* **2004**, *4*, 2467–2471.
(14) Truong, T. T.; Lin, R. S.; Jeon, S.; Lee, H. H.; Maria, J.; Gaur, A.; Hua, F.; Meinel, I.; Rogers, J. A. *Langmuir* **2007**, *23*, 2898–2905.
(15) Malyarchuk, V.; Hua, F.; Mack, N. H.; Velasquez, V. T.; White, J. O.; Nuzzo, R. G.; Rogers, J. A. *Optics Express* **2005**, *13*, 5669–5675.
(16) Taflove, A.; Hagness, S. *Computational Electrodynamics: The Finite-Difference Time-Domain Method*, Third Edition; Artech House Publishers, 2005.
(17) Chang, S.-H.; Gray, S. K.; Schatz, G. C. *Optics Express* **2005**, *13*, 3150–3165.
(18) Gray, S. K.; Kupka, T. *Phys. Rev. B* **2003**, *68*, 045415.
(19) Lee, T. W.; Gray, S. K. *Opt. Express* **2005**, *13*, 9652–9659.
(20) Johnson, P. B.; Christy, R. W. *Phys. Rev. B* **1972**, *6*, 4370–4379.
(21) McMahon, J. M.; Henzie, J.; Odom, T. W.; Schatz, G. C.; Gray, S. K. *Opt. Express* **2007**, *15*, 18119–18129.
(22) Rindzevicius, T.; Alaverdyan, Y.; Dahlin, A.; Hook, F.; Sutherland, D. S.; Kall, M. *Nano Lett.* **2005**, *5*, 2335–2339.
(23) Dahlin, A.; Zach, M.; Rindzevicius, T.; Kall, M.; Sutherland, D. S.; Hook, F. *J. Am. Chem. Soc.* **2005**, *127*, 5043–5048.
(24) McFarland, A. D.; Van Duyne, R. P. *Nano Lett.* **2003**, *3*, 1057–1062.
(25) Brolo, A. G.; Gordon, R.; Leathem, B.; Kavanagh, K. L. *Langmuir* **2004**, *20*, 4813–4815.
(26) Prikulis, J.; Hanarp, P.; Olofsson, L.; Sutherland, D.; Kall, M. *Nano Lett.* **2004**, *4*, 1003–1007.
(27) Kelf, T. A.; Sugawara, Y.; Cole, R. M.; Baumberg, J. J.; Abdelsalam, M. E.; Cintra, S.; Mahajan, S.; Russell, A. E.; Bartlett, P. N. *Phys. Rev. B* **2006**, *74*, 245415.
(28) Teperik, T. V.; Popov, V. V.; de Abajo, F. J. G. *Phys. Rev. B* **2004**, *69*, 155402.
(29) Raether, H. *Surface Plasmons on Smooth and Rough Surfaces and on Gratings*; Springer: New York, 1988.
(30) Maier, S. A. *Plasmonics: Fundamentals and Applications*; Springer: New York, 2007.
(31) Conn, A. R.; Scheinberg, K.; Vicente, L. N. *Math. Program., Ser. B* **2008**, *111*, 141–172.
(32) Powell, M. J. D. *Math. Program., Ser. B* **2002**, *92*, 555–582.

JP9024552